Table of Contents

Partial Volume Effect Correction using Anisotropic Backward Diffusion

Zsolt Márta and László Szirmay-Kalos

Budapest University of Technology and Economics
zsolt.marta@hivenet.hu, szirmay@iit.bme.hu

Abstract. This paper proposes an algorithm for correcting Partial Volume Effect in Positron Emission Tomography (PET) images, using registered Computed Tomography (CT) data to enhance the blurred PET image. The algorithm is based on a forward-and-backward anisotropic heat equation solver, deblurring the PET image along CT gradients. A forward diffusion force is also utilized to stabilize the process where necessary. The algorithm retains average original PET intensity avoiding the introduction of negative PET values, a crucial property in clinical uses. We implemented the algorithm for GPU and tested it with real measured PET/CT data.

1 Introduction

Positron Emission Tomography (PET) has the potential to produce quantitatively accurate measurements of tracer concentrations in vivo [15]. However, it has a limited spatial resolution and the reconstructions are blurred and rather noisy if radiation dose should be limited, which is always the case in clinical practice [14]. The direct consequence of limited resolution is the loss of signal for structures partially occupying the Point-Spread Function (PSF) of the scanner, i.e., with dimensions smaller than about 2-3 times its $FWHM$ [11]. This effect is usually referred to as Partial Volume Effect (PVE).

PET/CT systems allow simultaneous acquisition of PET and CT data. Hence the idea arises to enhance the blurry PET image with CT information. The main assumption is that tissue boundaries appearing in both images enables correction relying on anatomical data. This assumption seems realistic as different tissue types have different density (thus different intensity in CT scan), and also the radiotracer density depends on the tissue type. Therefore on the boundaries of different tissues, it is assumed that both CT and PET values change and thus CT and PET boundaries are co-located.

There are multiple approaches to correct PVE [2, 13, 5, 12, 3, 1, 15], although they usually require some a priori information about the scanner, or pose impractical assumptions. Popular methods that incorporate high-resolution anatomical information in the PET image are based on a multi-resolution image fusion approach, assuming that the gray levels in the high-resolution image must be positively correlated with those of the functional image to be corrected for PVE [15]. As pointed out in our earlier work, this assumption may be implausible [8].

The rest of the article is organized in the following way: first, Section 2 presents a short introduction to diffusion processes, particularly anisotropic diffusion along with previous works. Then, in Section 3 we propose our backward diffusion process, followed by the discussion of our stabilization method, and the combination of the two processes. Later, we discuss medical criteria and a modification to our algorithm in Section 3.3. Finally implementation details and results are presented and conclusions are drawn.

2 Anisotropic Diffusion

Partial Differential Equations have been widely studied and applied in the field of image processing in the past decades. A particular application area is image denoising and enhancement. The simplest denoising diffusion process [7] solves the heat equation in the form

$$\frac{\partial x}{\partial t} = \nabla^2 x \tag{1}$$

where x is an N-dimensional scalar function over the image domain. Solving this equation is equivalent to a convolution with a Gaussian kernel, and thus it filters the image uniformly. This uniformity causes unnecessary loss of information in addition to noise removal [17, Ch. 1.2]

To overcome this limitation, an edge-preserving non-linear diffusion process was first introduced by Perona and Malik [10]. Here, the diffusion process is controlled by a diffusion coefficient. They chose this coefficient a decreasing function of the image gradient, slowing down the smoothing near edges. The Perona-Malik equation is

$$\frac{\partial x}{\partial t} = \nabla \cdot \left(g\left(\|\nabla x\| \right) \nabla x \right) \tag{2}$$

with a monotone decreasing diffusivity function $g(s)$, such as

$$g(s) = \frac{1}{1 + \left(\frac{s}{\lambda}\right)^2}. \tag{3}$$

A further extension of the diffusion process applies a tensor which controls the flux of the process instead of a scalar-valued diffusivity coefficient. In certain applications it would be desirable to bias the flux towards the orientation of interesting features, avoiding the removal of these. The equation becomes then

$$\frac{\partial x}{\partial t} = \nabla \cdot \left(D \cdot \nabla x \right), \tag{4}$$

with the diffusion tensor D, a positive definite symmetric matrix. The Perona-Malik process can be extended to reduce noise near edges without destroying them. The diffusion tensor is chosen in a way that it prefers diffusion along edges to diffusion perpendicular to them.

Diffusion processes can also be used for image deblurring and enhancement. A method proposed by Gilboa et al. [6] simultaneously sharpens and denoises

the image while locally varying the diffusion coefficient. Their algorithm switches between a backward and a forward diffusion process based on the image gradient. The backward process is basically solving the heat equation (Eq. 2) backwards in time, simply having a negative diffusion coefficient. As the forward diffusion process is a convolution with a Gaussian kernel, similarly the backward diffusion can be described as a deconvolution operation. The process can be imagined as pushing PET values upward along "slopes", emphasizing gradients. As pointed out in their work, this backward diffusion process is highly unstable, and they use a custom diffusivity function to overcome this, combining a forward and a backward diffusion force in a single process.

3 Proposed Method

Our main objective is to sharpen the blurry PET image, enhancing the edges present in it, by using the registered anatomical data. Therefore, we use a backward diffusion process stabilized with a forward process. Our method works in arbitrary dimensions, but as medical data is usually in 3D, we present the implementation only in 3D.

3.1 The Backward Process

For the edge-enhancement we use an anisotropic backward diffusion process. To introduce high-frequency anatomical (CT) information in the PET image, we bias the sharpening process by CT edges. To do so, we define our diffusion tensor based on CT gradients. Let $\nabla\hat{y} = \frac{\nabla y}{\|\nabla y\|}$, then we define the tensor as

$$D_{\hat{y}} = \rangle\nabla\hat{y}, \nabla\hat{y}\langle = \nabla\hat{y}^{\mathsf{T}} \cdot \nabla\hat{y},$$

where y is the anatomical gray-value function, and $\rangle\cdot,\cdot\langle$ is the outer product in the Euclidean space. This dyadic tensor has eigenvalues $\lambda_1 = 1$ with corresponding eigenvector parallel to the CT gradient, and $\lambda_2 = \lambda_3 = 0$ with corresponding eigenvectors perpendicular to the CT gradient. This tensor is then used in Eq. 4. Here, PET gradients parallel to CT gradients are preferred, so the sharpening process enhances them more effectively. This way, PET intensity flows through CT gradients, creating PET edges along the CT ones. However, as there is no force to compensate the sharpening effect, PET values converge into extremities disregarding actual tissue boundaries. This can be seen intuitively, as slopes become steeper, the same amount of activity confines to a smaller region determined by PET distribution and not CT edges.

3.2 Stabilization

Our goal is to enhance tissue boundaries instead of just sharpening the PET image, and to approximate original positron activity in those regions. Therefore, a stabilization force is required to slow down or reverse the enhancement process

if PET regions shrink below tissue boundaries. In order to stabilize the backward diffusion process, we combine the sharpening process with a forward one. Hence, two opposing forces are applied, a sharpening backward diffusion along CT edges, and a simple forward diffusion force to stabilize PET regions.

We combine the two forces in one process by a linear combination of their corresponding tensors. The forward diffusion has the identity matrix as its tensor (resulting in Eq. 1). We determine the strength of the two forces by local features explained in this section. Our combined process now has the form

$$\frac{\partial x}{\partial t} = \nabla \cdot \Big((\lambda_{\hat{y}} D_{\hat{y}} + \lambda_I I) \cdot \nabla x \Big). \tag{5}$$

This combination benefits from both the edge-enhancement and region-stabilizing processes, leading to improved PET regions along tissue boundaries.

To create PET edges along tissue boundaries, we aim to create PET gradients co-located with CT ones. Therefore, we classify local features based on the gradients' magnitudes. Intuitive analysis shows four primary cases:

- *High PET gradient magnitude with high CT gradient magnitude.* In this case, PET edges are already strong along CT ones, so the algorithm should no further sharpen the image. Both processes should slow down.
- *Low PET gradient magnitude with high CT gradient magnitude.* Here, more sharpening is required to enhance edges, so the backward force should be emphasized.
- *High PET gradient magnitude with low CT gradient magnitude.* This occurs when PET edges are falsely created where no tissue boundary is present. This may be due to over-sharpening, or reconstruction noise. In this case, the stabilizing process should have greater emphasis.
- *Low PET gradient magnitude with low CT gradient magnitude.* Here, the process should not affect the image, as these conditions are present within tissues in normal case.

Based on these cases we derive two functions scaling the two opposite force. To obtain stability and visually satisfying results, these two functions must be continuous and differentiable over the positive real domain. The scaling function for the backward process should be monotone increasing in the CT gradient magnitude and decreasing in the PET gradient magnitude. The scaling function of the forward process should behave the opposite way. To scale the processes according to the magnitude of gradients we use a smoothed step function, for example, $\operatorname{sstep}(s) := \frac{2}{\pi}\arctan(s)$. Then the parameters $\lambda_{\hat{y}}$ and λ_I in Eq. 5 are replaced with the functions

$$\begin{aligned} f_{\hat{y}}\left(\|\nabla x\|, \|\nabla y\|\right) &:= \left(1 - \operatorname{sstep}\left(\|\nabla x\|\right)\right) \operatorname{sstep}\left(\|\nabla y\|\right), \\ f_{\hat{I}}\left(\|\nabla x\|, \|\nabla y\|\right) &:= \operatorname{sstep}\left(\|\nabla x\|\right) \left(1 - \operatorname{sstep}\left(\|\nabla y\|\right)\right). \end{aligned}$$

Notice that the scaling functions have an *implicit* effect on the diffusivity as their sum is not always 1, so they control the overall process speed as well as the ratio of the two forces.

To control image smoothness, we introduce a parameter to maximize the value of the forward scale function. With this parameter, we can determine the ratio of the two force, and thus the extent of PET regions compared to actual tissue sizes. The larger the forward process scale, the more space is filled with PET intensity and the smoother the image is. Our system equation becomes

$$\frac{\partial x}{\partial t} = \nabla \cdot \left(\left((1-\mu)\, f_{\hat{y}} D_{\hat{y}} + \mu f_I I \right) \cdot \nabla x \right). \tag{6}$$

Note that the scaling function parameters are omitted for simplicity.

3.3 Meeting Medical Criteria

PET is a quantitative measurement method, which means image intensities hold essential information about the tissue being analyzed. Obviously, negative values are invalid, so they should be avoided. Moreover, local average intensity needs to be retained as it holds crucial information.

To avoid negative values, we introduce an *explicit* diffusivity function. Negative values are a result of over-sharpening as the lower parts of the sharpened edge become negative. This effect is to be avoided, and thus we slow down and completely stop the process as values approach the zero boundary. We use a low value cut-off function to gradually slow down the diffusion processes for small PET values:

$$\text{lowcutoff}\,(x) := \begin{cases} \frac{x^2}{1+x^2} & \text{if } x \geq 0, \\ 0 & \text{if } x < 0. \end{cases}$$

It can be easily seen that this function makes the diffusivity smoothly diminish at low PET values.

It is not enough to simply scale the divergence value in Eq. 6, because it would not scale symmetrically the diffusion process, leading to incorrect values, especially regarding local average intensity. So we must scale gradients instead. As the gradient in a point is affected by the local infinitely small neighborhood of that point, we must take the PET values of that neighborhood into account. Taking the minimum of the neighboring PET values clearly suffices to stop the diffusion process as soon as intensities approach the zero-boundary. As the partial derivatives are affected by points along each axes, only those must be considered. So the diffusivity function defined in the N-dimensional image space, at point i_0 becomes

$$\text{diffity}\,(i_0) := \text{lowcutoff}\left(\min \bigcup_{n=1}^{N} \{\xi_n^+\,(i_0)\,, \xi_n^-\,(i_0)\} \right),$$

where

$$\xi_n^{\pm}\,(i_0) := \lim_{\Delta \to 0, \Delta \neq 0} \left(x\left(i_0 + e_n^{\pm \Delta} \right) \right),$$

and e_n^{Δ} is a vector with $e_n^{\Delta} = \Delta$ in the n-th position, and 0 elsewhere. Inserting functional d into Eq. 6, the system equation becomes

$$\frac{\partial x}{\partial t} = \nabla \cdot \left(d \left((1-\mu) f_{\hat{y}} D_{\hat{y}} + \mu f_I I \right) \cdot \nabla x \right). \tag{7}$$

This way we have avoided negative values by stopping the diffusion as soon as PET intensities approach the negative domain.

There is no well-established theory of general non-linear anisotropic diffusion methods, except for some simpler cases [16, 17]. As Weickert [17, pp. 63-64] pointed out, certain types of anisotropic diffusion processes retain average grey value. This requires well-posedness, which is not guaranteed in our case. However, due to the stabilization and similarity to the forward problem based on divergence-form and the smooth scaling functions, we expect that the average gray level is not divergent. This is examined empirically in Section 5.

4 Implementation

Our proposed method is implemented and tested in 3D as it is the usual dimension of medical data. We solve Eq. 7 using a forward Euler time-marching scheme, and use central differences spatial differentiation. First, we scale the PET image to the (presumably) larger CT image size by a simple tri-cubic filter on the GPU. We iterate until there is no significant change in the image, when we have approached the steady-state solution well enough. This is measured using the sum of absolute difference between each subsequent image:

$$\mathrm{diff}\left(x^t, x^{t+1}\right) := \sum_{i \in \Omega} |x^t\,(i) - x^{t+1}\,(i)\,|,$$

where x^t is the PET image after iteration t ($t = 0$ gives the initial PET image), and $i \in \Omega$ is a point in the image space. When this difference falls below a threshold, we stop iterating. To determine this threshold independently from the actual image, we use the first difference, i.e. $\mathrm{diff}\left(x^0, x^1\right)$ as a unit, and define the stopping condition as

$$\mathrm{diff}\left(x^t, x^{t+1}\right) \leq \epsilon \cdot \mathrm{diff}\left(x^0, x^1\right).$$

Obviously, larger ϵ leads to coarser, less sharpened image.

As for the force functions, in order to maximize their effect we scale gradients using the mean gradient magnitudes. Defining

$$\mathrm{MGM}\left(\nabla x\right) = \frac{1}{\|\Omega\|} \sum_{i \in \Omega} \|\nabla x\,(i)\,\|,$$

we get

$$\mathrm{sstep}^{(2)}\left(\nabla x\right) := \frac{2}{\pi} \arctan\left(\frac{\|\nabla x\|}{\mathrm{MGM}\left(\nabla x\right)} \right).$$

The CT gradient case is analogous. Clearly, the step function will take 1/2 on average-size gradients; a normal distribution of gradient magnitudes assumed, this way our step function maximizes the spread of scaling values.

We have implemented the Euler-scheme on the GPU, using OpenCL and C++. Voxel intensity calculations are inherently massively parallelizable, and hence the algorithm can be implemented efficiently.

5 Results

We tested the proposed algorithm using two real measured data. The first one is a mouse measurement, the CT image size is $217 \times 211 \times 528$, and the PET image size is $136 \times 132 \times 330$ (Data courtesy of P. Blower, G. Mullen, and P. Mardsden, Rayne Institute, King's College, London). We ran our method for multiple μ and ϵ values. Corresponding line profiles are shown in Fig. 3. As explained earlier, lower μ values increase sharpness and decrease residual intensity between tissues, making them more confined. On the other hand, they introduce more noise. Larger ϵ values cause the process to stop before reaching maximum sharpness (based on μ). As seen in Fig. 1, too small μ values cause tissues not to be filled correctly as well as more CT noise added to the image, and too large μ values leave more intensity spilled out by PVE. Tables 1 and 2 show running time statistics of the measurements with different μ values. Notice that the less smooth image is produced, the less time it takes to converge, and the less the difference from the original image will be due to less sharpening. Also, running time is much lower than that of the typical PET reconstruction. The error curve is depicted in Fig. 5. Notice the visible convergence of differences. Average gray-value is not constant, although it seems converging to an approx. 1.25% change, which is acceptable.

Our other measurement is a Derenzo phantom of rod diameters in 0.7mm – 1.2 mm with CT image size $333 \times 333 \times 281$, and PET image size $173 \times 173 \times 146$ (image created with Mediso Ltd.'s NanoPET/CT [9]). It is a quite noisy measurement, but our algorithm can still achieve improvement compared to the original PET image. As seen in Fig. 4, small μ values lead to noisy results, but the rods have more significant contour. Fig. 2 shows the original images and two results. Notice that small rods became more observable. As before, less sharpening causes the algorithm to converge in fewer iterations.

μ	0.01	0.05	0.1
Time (m:s)	8:27	7:47	5:34
Iter. cnt.	1110	1025	716
Diff	83.32%	63.25%	49.89%

Table 1. Running times of the mouse measurement with different μ values ($\epsilon = 0.05$).

μ	0.01	0.05	0.1
Time (m:s)	10:09	7:11	6:44
Iter. cnt.	1096	764	713
Diff	61.89%	30.7%	25.92%

Table 2. Running times of the Derenzo measurement with different μ values ($\epsilon = 0.05$).

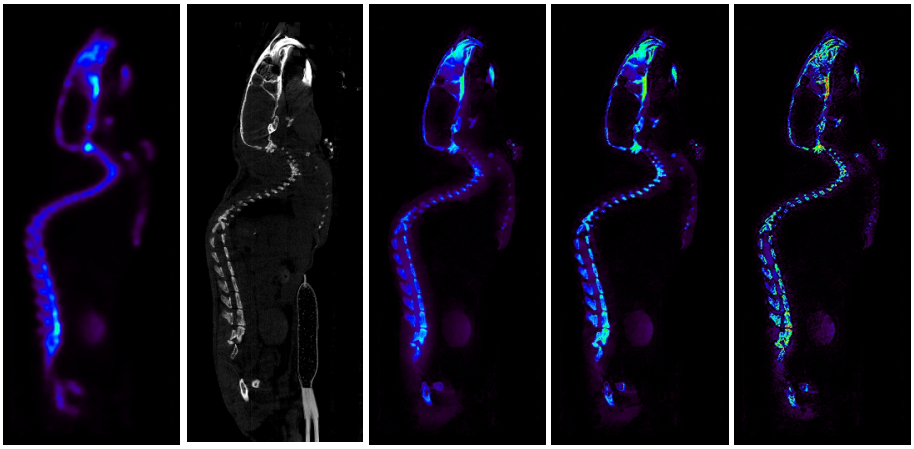

Fig. 1. Original PET mouse image, registered CT data, and upgraded images for different μ values, $\mu = 0.1$, $\mu = 0.05$, $\mu = 0.01$. Data courtesy of P. Blower, G. Mullen, and P. Mardsden, Rayne Institute, King's College, London.

6 Conclusion

We proposed an algorithm for Partial Volume Effect correction for PET reconstruction using registered CT data. Our method is a combination of a backward anisotropic diffusion and a forward diffusion process. Their combination is based on local gradient magnitudes. Additional conditions are applied to meet medical criteria. We implemented our method for GPU-s, and tested it with real-world examples. Results show that our method effectively sharpens the PET image, creating edges on tissue boundaries, as well as retaining structural and functional

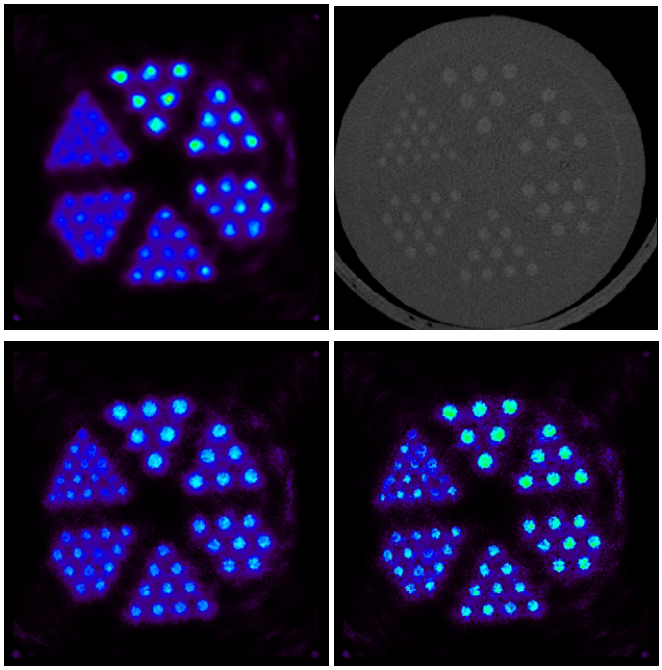

Fig. 2. Original PET (top left), CT (top right), and two results (bottom) of the Derenzo measurement, with $\mu = 0.1, \epsilon = 0.05$ (bottom left) and $\mu = 0.05, \epsilon = 0.05$ (bottom right) parameter values. Data courtesy of Mediso Ltd. [9]

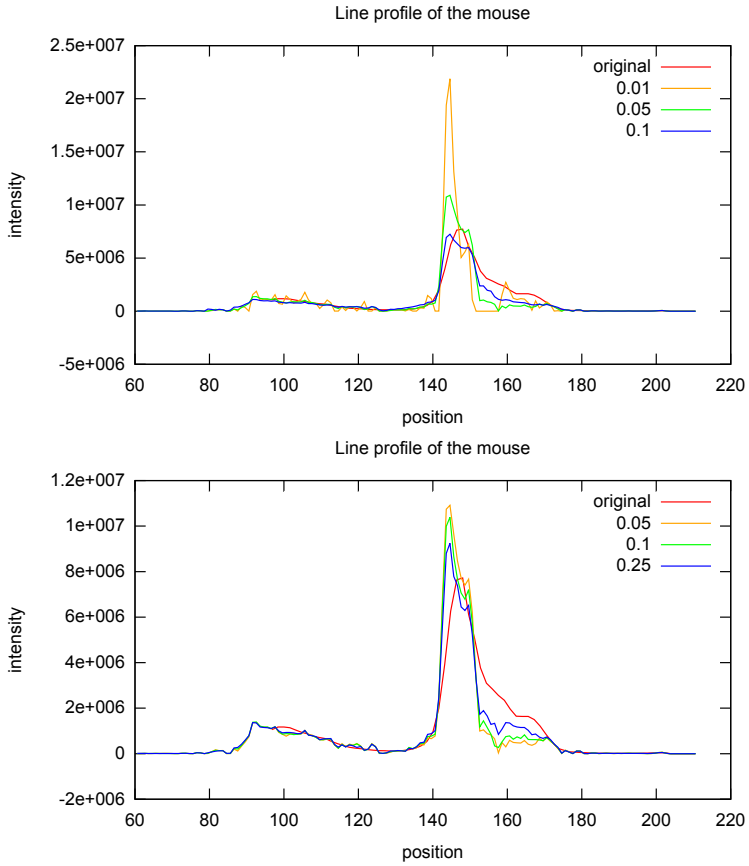

Fig. 3. Line profiles of the mouse measurement for different μ ($\epsilon = 0.05$) (top) and ϵ ($\mu = 0.05$) (bottom) parameter values.

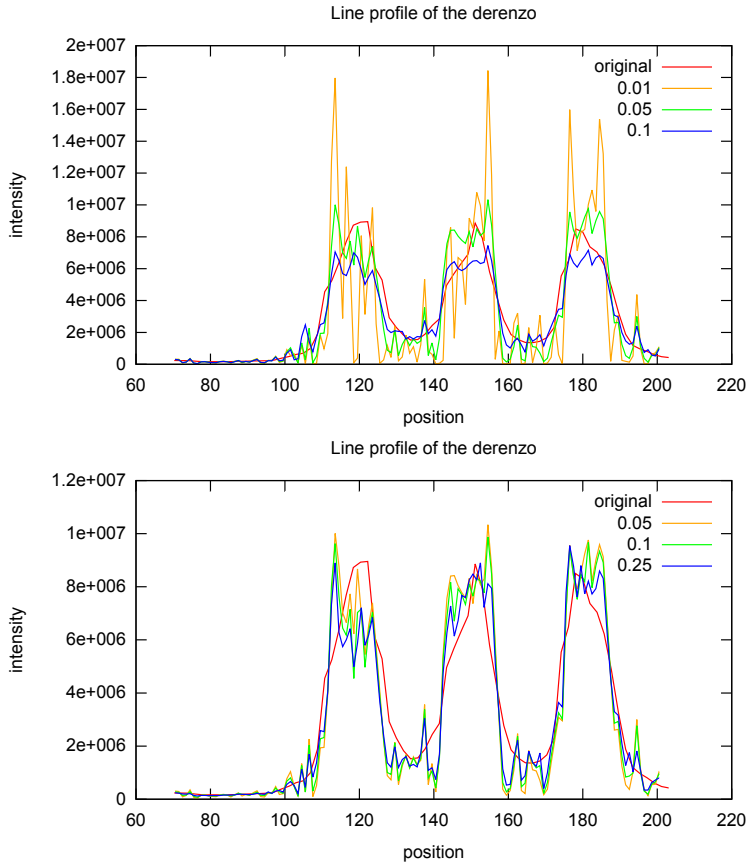

Fig. 4. Line profiles of the Derenzo measurement for different μ ($\epsilon = 0.05$) (top) and ϵ ($\mu = 0.05$) (bottom) parameter values.

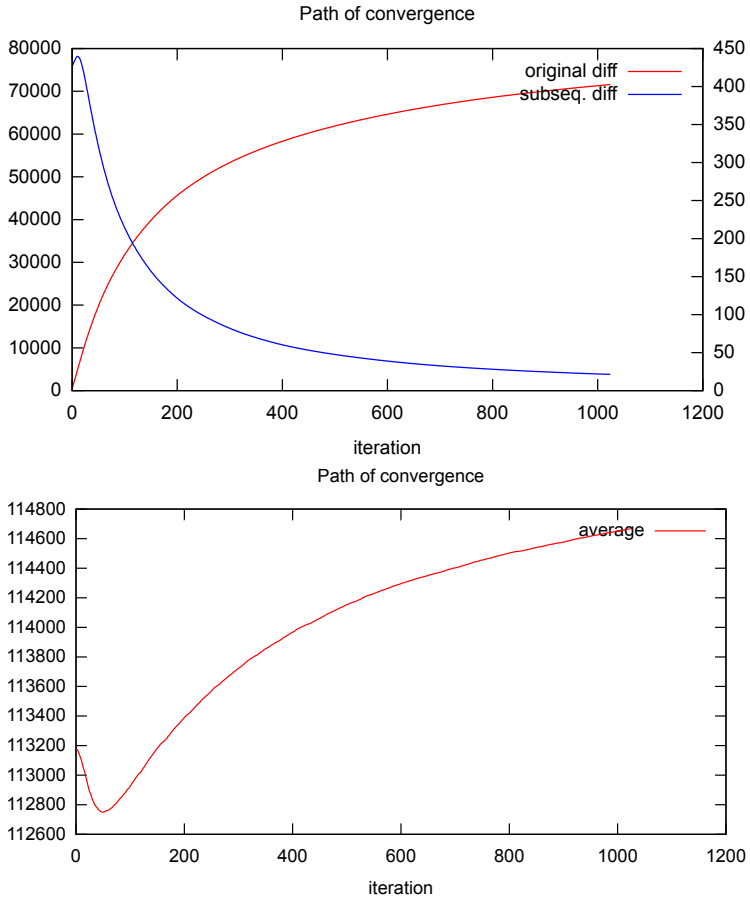

Fig. 5. Path of convergence for the mouse measurement, $\mu = 0.05, \epsilon = 0.05$. Absolute differences (top) and average gray-value (bottom).

information. Even in quite noisy circumstances, our algorithm can achieve improvement over the original PET image. This enhancement procedure is expected to be part of the PET reconstruction code of the TeraTomo^{TM} program [4].

Acknowledgements

This work has been supported by the TeraTomo project of the National Office for Research and Technology, TÁMOP-4.2.2.B-10/1-2010-0009, and OTKA K-104476.

References

1. David L. Barbee, Ryan T. Flynn, James E. Holden, Robert J. Nickles, and Robert Jeraj. Partial volume correction of PET-imaged tumor heterogeneity using expectation maximization with a spatially varying point spread function. *Phys. Med. Biol.*, 55:221–236, 2010.
2. N. Boussion, M. Hatt, F. Lamare, Y. Bizais, A. Turzo, C. Cheze-Le Rest, and D. Visvikis. A multiresolution image based approach for correction of partial volume effects in emission tomography. In *Phys. Med. Biol.*, pages 1857–1876, 2006.
3. Kjell Erlandsson, Irene Buvat, P. Hendrik Pretorius, Benjamin A. Thomas, and Brian F. Hutton. A review of partial volume correction techniques for emission tomography and their applications in neurology, cardiology and oncology. *Phys. Med. Biol.*, 57:119–159, 2012.
4. M. Magdics et al. TeraTomo project: a fully 3D GPU based reconstruction code for exploiting the imaging capability of the NanoPET/CT system. In *World Molecular Imaging Congress*, 2010.
5. Francisca P. Figueiras, Xavier Jimenez, Deborah Pareto, and Juan D. Gispert. Partial volume correction using an energy multiresolution analysis. In *IEEE Nuclear Science Symposium Conference Record*, pages 2724–2727, 2009.
6. Guy Gilboa, Nir Sochen, , and Yehoshua Y. Zeevi. Forward-and-backward diffusion processes for adaptive image enhancement and denoising. In *IEEE Trans on Image Processing*, volume 11. 2002.
7. I. Kopilovic and T. Szirányi. Artifact reduction with diffusion preprocessing for image compression. *OPTICAL ENGINEERING*, 44, 2005.
8. Zsolt Márta. Partial volume effect correction on the GPU. In *Proceedings of CESCG 2012: The 16th Central European Seminar on Computer Graphics*, 2012.
9. Mediso. NanoScan PET/CT in-vivo preclinical imager. http://www.mediso.hu/products.php?fid=2,11&pid=86.
10. Pietro Perona and Jitendra Malik. Scale-space and edge detection using anisotropic diffusion. In *IEEE Trans on Pattern Analysis and Machine Intelligence*, volume 12, pages 629–639. 1990.
11. Olivier G. Roussel, Yilong Ma, and Alan C. Evans. Correction for partial volume effects in PET: Principle and validation. *Journal of Nuclear Medicine*, 39:904–911, 1998.
12. W. Paul Segars, Benjamin M. W. Tsui, A. J. Da Silva, and L. Shao. CT-PET image fusion using the 4D NCAT phantom with the purpose of attenuation correction. In *2002 IEEE Nuclear Science Symposium Conference Record*, pages 1775–1779, 2003.

13. Miho Shidahara, Charalampos Tsoumpas, Alexander Hammers, Nicolas Boussion, Dimitris Visvikis, Tetsuya Suhara, Iwao Kanno, and Federico E. Turkheimer. Functional and structural synergy for resolution recovery and partial volume correction in brain PET. *Elsevier NeuroImage*, 44:340–348, 2009.
14. Arne Skretting. Intensity diffusion is a better description than partial volume effect. *Eur J Nucl Med Mol Imaging*, 36:536–537, 2009.
15. Marine Soret, Stephen L. Bacharach, and Irène Buvat. Partial-volume effect in PET tumor imaging. *Journal of Nuclear Medicine*, 48:932–945, 2007.
16. Joachim Weickert. Theoretical foundations of anisotropic diffusion in image processing. In *Computing, Suppl. 11*, pages 221–236. 1996.
17. Joachim Weickert. *Anisotropic Diffusion in Image Processing.* B.G. Teubner Stuttgart, 1998.